Microfluidics and Nanofluidics (2020) 24:52
https://doi.org/10.1007/s10404-020-02356-0

RESEARCH PAPER

Acoustofluidic microdevice for precise control of pressure nodal positions

Sinan Yigit[1] · Han Wang[2] · Song-I. Han[1] · Younghak Cho[3] · Arum Han[1,4]

Received: 29 February 2020 / Accepted: 1 June 2020 / Published online: 16 June 2020

Abstract

Acoustic wave-based manipulation of cells and particles in microfluidic channels has gained wide popularity in the past decade since it provides label-free and contact-less manipulation of them in a microfluidic environment using a very simple microfluidic structure and experimental setup. In bulk acoustofluidics, an acoustic resonance field that generates an acoustic standing wave within a microfluidic channel creates acoustic pressure nodes and anti-nodes, to which particles migrate to or migrate away from. However, in a given straight microfluidic channel, the position of the acoustic pressure nodes and anti-nodes are fixed and cannot be changed along the channel, limiting more diverse capabilities in moving particles and cells to a desired location within a microfluidic channel. Here, an acoustic echo-channel where its width changes along the flow direction was created right next to the main flow channel separated by a thin wall that minimizes the disturbance of the acoustic wave. This allows the location of the acoustic pressure nodes and anti-nodes to be controlled in the main flow channel depending on the width of the echo-channel, hence providing more flexibility in manipulating particles and cells to a certain position within a given microfluidic channel. The capability to more freely manipulate particles and cells within a microfluidic channel further expands the application areas of bulk acoustofluidics.

Keywords Bulk acoustofluidics · Acoustic nodal position · Acoustic echo-channel · Multi-frequency acoustophoresis

1 Introduction

To date a variety of particle and cell manipulation techniques and applications have been developed using bulk acoustic wave (BAW)-based acoustofluidic systems (Antfolk and Laurell 2019; Park et al. 2016). The principle of these systems lies on the phenomena that particles passing through an acoustic resonance field, namely the acoustic standing wave created between two side channels of a microfluidic channel functioning as transversal resonators, move towards positions in the microfluidic channel called acoustic pressure nodes and/or anti-nodes, depending on the polarity of their acoustic contrast factors. Depending on the frequency applied through the piezoelectric transducer generating the acoustic wave, these acoustic pressure nodes are generated in the ½ position, ¼ and ¾ positions, and so on of the microfluidic channel width. The major benefits of bulk acoustofluidic technology is that it allows contactless and label-free manipulation of particles, including cells, in microscale with an extremely simple microstructure and instrument setup. Thanks to these benefits, this technology has been widely used in applications ranging from cell separation (Antfolk et al. 2015; Lenshof et al. 2012), oil droplet separation (Wang et al. 2014), cell property analysis (Ding et al. 2012; Wang et al. 2018; Wiklund et al. 2014), and cell trapping (Evander and Nilsson 2012), to name a few. Additionally, this technology has been combined with other available

Electronic supplementary material The online version of this article (https://doi.org/10.1007/s10404-020-02356-0) contains supplementary material, which is available to authorized users.

✉ Younghak Cho
yhcho@seoultech.ac.kr

✉ Arum Han
arum.han@ecen.tamu.edu

1 Department of Electrical and Computer Engineering, Texas A and M University, College Station, TX 77843, USA

2 Department of Biomedical Engineering, School of Medicine, Tsinghua University, Beijing 100084, China

3 Department of Mechanical System Design Engineering, Seoul National University of Science and Technology, 01811 Seoul, Republic of Korea

4 Department of Biomedical Engineering, Texas A and M University, College Station, TX 77843, USA

microfluidic technologies, such as droplet microfluidics (Destgeer et al. 2016; Fornell et al. 2015) and electrophoresis (Wiklund et al. 2006), for more complex assays to be performed in a microfluidic format.

To actuate bulk acoustofluidic microdevices, a piezoelectric transducer typically attached to the bottom of a microfluidic channel is excited at the resonant frequency that matches the acoustic wavelength of the width of the microchannel. At this resonant frequency, particles passing through the acoustic resonance field move towards the acoustic pressure nodes or anti-nodes based on their density and compressibility in comparison to those of the surrounding media. If the particles have a positive acoustic contrast factor, they move towards the acoustic pressure node where the amplitude of motion is zero. On the other hand, if particles have a negative acoustic contrast factor, they move towards the acoustic pressure anti-node where the amplitude of motion is maximum. This allows particle and cell manipulation to be conducted very easily. However, one of the biggest limitations of this technology is that the locations of the acoustic pressure nodes are fixed, in a sense that they can only be formed at the ½ (primary harmonic resonance) or ¼ & ¾ (secondary harmonic resonance) positions (or even 1/6 in the case of tertiary pressure nodes, but not commonly used as the force is quite weak) in a given microfluidic channel when the primary, secondary, and tertiary acoustic resonance frequencies are applied. Thus, this technology cannot be used to manipulate cells and particles freely to any position desired within a microfluidic channel, thus somewhat limiting its flexibility and application areas. More flexible capability in controlling the location of the acoustic nodal positions will enable changing the location of particles and cells inside a microchannel more freely, and make applications that require better control over the location of particle and cell migration in a given microchannel easier to be implemented.

The possibility of moving particles and cells to a position other than the fixed acoustic nodal lines through decoupling the physical microfluidic boundary from the acoustic wave boundary has been demonstrated previously (Leibacher et al. 2014). In that study, an acoustically transparent thin sidewall was created within the silicon microfluidic channel by filling part of the microfluidic channel with a polydimethylsiloxane (PDMS) structure, removed by laser cutting, so that the fluidic boundary created by the PDMS sidewall could be decoupled from the acoustic boundary created by the silicon microfluidic channel sidewall. This was possible because PDMS is relatively transparent to acoustic wave. By adjusting the width of this PDMS structure inside the silicon microfluidic channel, the effective position of the acoustic nodal position could be adjusted within the flow channel, where the actual acoustic nodal position is fixed by the two sidewalls of the silicon microchannel but the microfluidic channel width is reduced by the width of the PDMS structure within the microfluidic channel. Another reported method is the use of a bypass channel (also called echo-channel) adjacent to the main flow channel that allowed the acoustic pressure nodes and anti-nodes to be dynamically tuned depending on the property of medium filling the echo-channel (Jung et al. 2015). Here, the main flow channel was physically separated from the echo-channel by a thin side wall (less than 20 μm in width), making it almost transparent to the acoustic wave. Thus, the combined width of the main channel and the echo-channel becomes the effective channel width from acoustic wave perspective, while the flow channel width is defined by the walls of the main flow channel. By filling this echo-channel with medium having different densities, and thus changing the speed of sound wave, it was possible to create an acoustic pressure node in any location within the main channel. Although overcoming many limitations of conventional bulk acoustofluidics, changing the location of cells and particles along the flow direction of the channel is still not possible, as the locations of the acoustic pressure nodes are still fixed and cannot change along the flow direction of a microfluidic channel.

Here, we present a bulk acoustofluidic device where the echo-channel has different widths along the flow direction of the main channel, essentially changing the effective acoustofluidic channel width along the flow direction. This allows the position of the acoustic pressure node to change along the flow direction, enabling the location of particles and cells to change laterally as they flow through the main flow channel. This new method provides the first bulk acoustofluidic method that allows the position of particles and cells to change laterally as they move along the flow direction, and has the potential to further broaden the application areas of bulk acoustofluidics-based particle/cell manipulation.

2 Methods

2.1 Working principle

In wave theory, wavelength equals to the speed of wave times the frequency of the wave. In acoustofluidics, if the wavelength of the acoustic wave is adjusted to be equal to the microchannel width or multiples of the channel width, an acoustic resonance field is generated. If the channel width is equal to half of the acoustic wavelength, it means that the channel is in its fundamental (*λ/2*) resonance mode, and there will be one nodal plane created in the middle of the microchannel. Similarly, if the channel width is equal to the wavelength, the channel is in its first harmonic (*λ*) mode, and in this case, there will be two pressure nodal planes generated, one at the ¼ position and the other at the ¾ position within the channel (Fig. 1a).

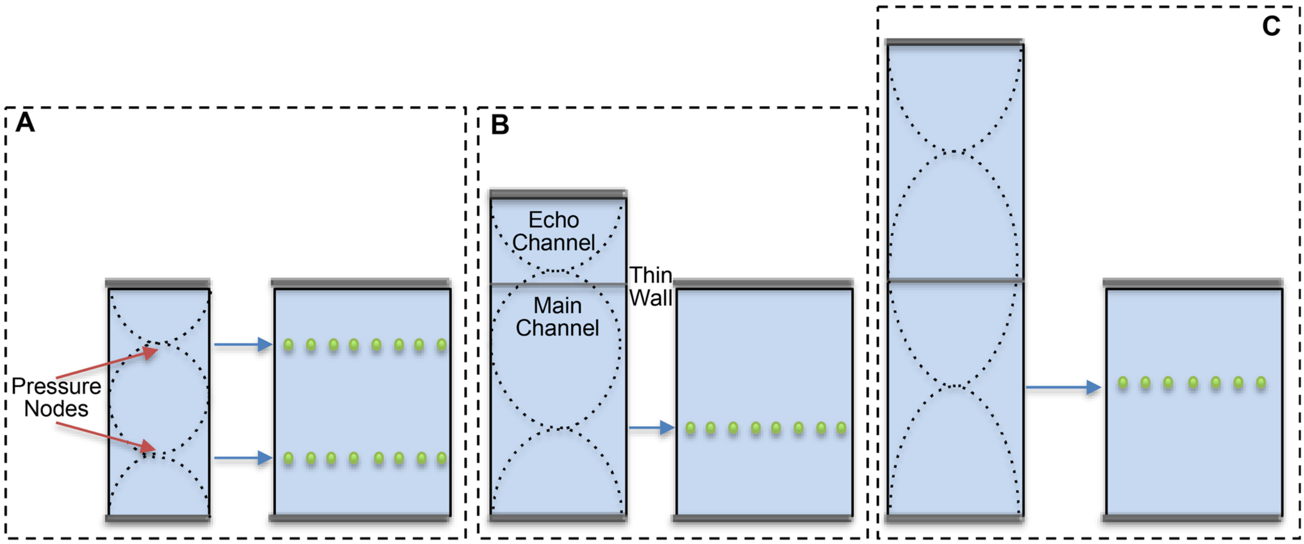

Fig. 1 **a** Nodal positions in a microfluidic channel when excited at the first harmonic mode. **b** Nodal positions in the microfluidic channel having a relatively narrow echo-channel separated by a thin wall and excited at the first harmonic mode. **c** Nodal positions in a microfluidic channel having a relatively wide echo-channel separated by a thin wall and excited at the first harmonic mode

If an echo-channel is added next to the main fluidic channel separated by a thin wall, the thin wall functions as a physical boundary for the flow itself but almost transparent to the acoustic wave. This makes the width of the combined main channel and the echo-channel as the effective channel width of the acoustic full wavelength resonator. Thus, from acoustofluidics perspective, the effective channel width W_{eff} can be defined by the following Eq. (1), which can be used to calculate the needed resonance frequency (Fong et al. 2014).

$$W_{\mathrm{eff}} = W_{\mathrm{main}} + W_{\mathrm{echo}}(C_w/C_{\mathrm{echo}}) + T_{\mathrm{wall}}(C_w/C_{\mathrm{Si}}) \tag{1}$$

In this equation, W_{eff} stands for the effective channel width from the acoustic wave perspective and as being the sum of the main channel width, W_{main}, and the scaled version of the echo-channel width, W_{echo}, and the scaled version of the thickness of the wall that separates the echo-channel and the main channel, T_{wall}. C_w is the speed of sound in the main flow channel and set as 1531 m/s (Haynes 2014). C_{echo} is the speed of sound inside the echo-channel, and set as 1496 m/s since deionized (DI) water was used in the echo-channel (Cushing et al. 2017). C_{Si} represents the speed of sound in silicon and the value was set to 8433 m/s (Hopcroft et al. 2010). The resonant frequency in the first harmonic mode was represented as f_1 and calculated by dividing the speed of sound in the microfluidic channel by the effective channel width. COMSOL Multiphysics™ software was also utilized to examine the effect of echo-channel width on the positions of the acoustic pressure nodes. The details of the numerical model are shown in the supplementary section. In that numerical study only 2D models have been employed. Here it might be considered that 3D models could be a better approach to characterize the nodal positions inside the microfluidic channel. However, it is thought that it will be a preliminary examination to provide an illustration for further studies. Further research can be implemented to understand the effect of boundaries and sharp edges of the microfluidic channel.

When the width of the echo-channel increases, the effective channel width also increases, which causes the nodal positions in the main channel to shift towards the echo-channel. If this device is actuated in its first harmonic (λ) mode, there will be two acoustic pressure nodal planes. The location of these planes can be adjusted using the echo-channel so that one nodal plane is formed inside the main flow channel and the other one formed inside the echo-channel, resulting in effectively only one pressure nodal plane to exist in the main flow channel. This phenomenon is very useful since in many applications, having two nodal planes that results in particles or cells moving to two different locations inside the flow channel is not desired. This concept is summarized in Fig. 1. It might be considered that solid partition might be unnecessary since laminar flow can be used in microfluidic channels since there are plenty of immiscible fluids. However, there has been studies showing that immiscible fluids can be mixed by the help of acoustofluidics (Yeo and Friend 2009; Pothuri et al. 2019). At certain frequencies the laminar flow can be distorted, and this situation is not desirable in most of the microfluidic experiments. To keep two fluids separated a solid partition is very advantageous by moving the particle/cells to nodal positions while keeping the two different fluids separated.

To test this proposed concept, microfluidic devices with different main channel and echo-channel widths were tested. In the first design, the main channel width was 1600 µm and the echo-channel widths varied from 678 µm to 2678 µm, giving an expected acoustic resonance frequency range between 350 and 660 kHz. In the second set of designs, the main channel width was reduced to 800 µm to increase the frequency range to be tuned between 840 kHz and 1.31 MHz to avoid possible overlapping of the resonant frequencies. For example, when the echo-channel width is 1078 µm, the expected resonant frequency is 0.56 MHz, which is very close to 0.55 MHz, the resonant frequency when the echo-channel width is 1478 µm. In these two sets of design, the wall thickness that separates the main flow channel and the echo-channel was fabricated to be ~ 10 µm. Finally, an echo-channel where the width changed from 1800 to 1000 and then to 300 µm, shaped like a staircase along the flow direction, was designed. In this design, the wall thickness was increased to 20 µm to avoid potential liquid leakage issue between the two adjacent channels.

2.2 Microdevice fabrication

The acoustofluidic microdevices were fabricated by the following steps. First, the microfluidic channel designs were patterned by photolithography to define the 1 µm thick etch mask on a silicon wafer and then etched into the silicon substrate using deep reactive ion etching (DRIE) to a depth of 105 µm. Fluidic access holes were drilled in a 500 µm thick borosilicate glass layer using a diamond-plated drill bit mounted on a bench top drill press (DP101, Ryobi Ltd, SC). The glass and silicon layer were anodically bonded at 400 °C by applying 700 V of DC voltage for 40 min. After the bonding process, ferrules were glued onto the holes of the glass layer using epoxy for fluidic access. Tygon tubings (VWR, USA) were inserted inside the ferrules and sealed with epoxy. The PZ26 type PZT (Ferroperm, Denmark) was bonded to the bottom of the microfluidic chip with cyanoacrylic glue (Loctite, USA), and wires were soldered to the PZT for electrical interconnect. Photograph of one of the fabricated devices can be seen in the supplementary information where the PZT transducer is attached onto the back of the microdevice.

2.3 Acoustofluidic device testing

Acoustofluidic device testing was conducted under an upright microscope (Eclipse LV100D, Nikon, Inc.) and microparticles suspended in fluids were flown through the microchannels by a 4-barrel syringe pump (Fusion 400, Chemyx, Inc., MA). The flow rate was chosen to be 500 µL/h. Fluorescent polystyrene microspheres (Thermoscientific, CA, USA) mixed with de-ionized (DI) water was used for all experiments for easy visualization of particle movement. For devices with the straight echo-channel design (single width throughout the length of the microchannel), a function generator (DG4202, Rigol Technologies Inc, USA) was utilized to generate a sinusoidal signal that was amplified through a 50-dB power amplifier (2100L, E&I, Ltd.) and applied to the PZT. For the chip with changing echo-channel width, a LabVIEW™ (National Instruments, TX, USA) program was developed to generate sums of two sinusoidal signals from a function generator (AFG3021B, Tektronix Inc, USA). This signal was then applied to the PZT through a 50-dB power amplifier (2100L, E&I, Ltd.).

3 Results and discussion

3.1 Straight echo-channel devices

The first attempt was to determine whether the acoustic pressure and anti-pressure nodal positions can be successfully changed in a microfluidic channel using echo-channels having different channel widths. For this purpose, two different designs of acoustofluidic devices were tested. In the first set of chips, the main channel width was selected to be 1600 µm and the wall thickness was microfabricated to be 10 µm. In Table 1 all the results of experiments done with the first set of chips are summarized.

In all cases, the width of the main channel is 1600 µm and wall thickness is 10 µm. Overall, as the echo-channel becomes wider, it can be seen that the particle focusing

Table 1 Summary of the various echo-channel widths and corresponding parameters tested. In all cases, the width of the main channel is 1600 µm and wall thickness is 10 µm.

Channel characteristics (µm)					Calc. freq (MHz)	Real freq (MHz) & Vpp
W_{main}	W_{echo}	W_{eff}	$Calc.x_1$	$Real\ x_1$	f_1	f_1
1600	678	2280	570	527	0.66	0.68 (130 mV)
1600	1078	2680	670	676	0.56	0.60 (460 mV)
1600	1478	3080	770	751	0.49	0.55 (64 mV)
1600	2278	3880	970	873	0.39	0.42 (400 mV)
1600	2678	4280	1070	921	0.35	0.37 (400 mV)

positions can be successfully controlled from the 527 μm position to the 921 μm position (Fig. 2a). At the same time, it can also be seen that as the echo-channel becomes wider, the discrepancy between the calculated nodal position and the actual nodal position becomes larger. The error between the calculated and real resonance frequencies required to focus the particles to the nodal position is between 3 to 7% compared to the calculated values for the 1600 μm-wide acoustofluidic device (Fig. 2b).

Despite this success in proof of concept demonstration, as the echo-channel width increased, the frequency range that needs to be applied to focus the microparticles became narrower, and this narrow frequency range causes easy mismatching of the resonant frequencies. For example, when the echo-channel width is 1478 μm, the applied frequency that is needed to focus the particles was 16% off from the expected result. This analysis resulted in the realization that the frequency range should be broadened so that overlapping of corresponding frequencies for different echo-channel widths could be avoided. Overall, of the first set of chips tested, when the echo-channel widths were smaller than 1478 μm, the discrepancy between the expected and actual nodal positions was less than 50 μm. However, for larger echo-channel widths such as 2278 and 2678 μm, the discrepancy was much bigger (97 and 149 μm, respectively). In addition, as can be seen from Table 1, the expected and real resonant frequencies are very close to each other when the echo-channel widths are 2278 μm and 2678 μm, causing challenges in properly tuning the resonance frequency.

To overcome these challenges, in the second design the main channel width was reduced to 800 μm. By reducing the main channel width, the frequency range that can be used was broadened so that better frequency tuning, and hence nodal position tuning, could be achieved. Figure 3a shows the scanning electron microscopic (SEM) image of the microfabricated straight echo-channel device having a main-channel width of ~ 800 μm and echo-channel width of ~ 785 μm before the silicon channel was sealed with glass by anodic bonding. Following the sealing of the channel, this 800 μm-wide main-channels were tested using polystyrene microparticles. The brightfield images of different particle positions for the varying echo-channel widths are shown in Fig. 3b. As an example, a focused stream of polystyrene microspheres flowing ~ 302 μm away from the lower wall boundary when the echo-channel width is 450 μm can be seen in this figure. In this experiment, the frequency of the sinusoidal signal applied to the PZT was 1.26 MHz, and V_{pp} was set to 120 mV going into the power amplifier. When the echo-channel width increased to 975 μm, the location of the acoustic pressure nodal position moved to ~ 426 μm away from the lower wall boundary as shown in the same figure. For this case, the frequency of the applied signal was 0.83 MHz and V_{pp} going into the power amplifier was 180 mV.

One aspect to note here is that while running the experiments, some microparticles seem to be flowing into the side of the echo-channel in particular locations of the microchannel, suggesting that there are some leakages between the main channel and the echo channel. Therefore, some flow perturbations seem to be occurring in some part of the channel. This is most likely due to the fact that the wall separating the main channel and the side echo-channel to decouple the acoustic boundary is only 10 μm wide, thus not sufficient to completely seal the channel through the anodic bonding process. Due to this reason, for the subsequent step-shaped echo channel design, a wider wall thickness will be considered.

Overall, as shown in Fig. 3c, changing the echo-channel width from 975 μm to 343 μm when the main channel width is kept at 800 μm makes the acoustic pressure nodal positions to change from ~ 426 μm to ~ 276 μm. For instance, increasing the echo-channel width from 450 μm to 605 μm almost results in ~ 70 μm change in the acoustic pressure nodal position. When main channel width is closer to the echo-channel width, the calculated and actual resonant frequencies become closer to each other. This phenomenon can be seen in Fig. 3d.

The calculated and experimental nodal positions and their corresponding resonant frequencies for the different echo-channels are summarized in Table 2. Overall, it can be seen that this second set of devices (compared to that summarized in Table 1) provides a better predictability of the actual

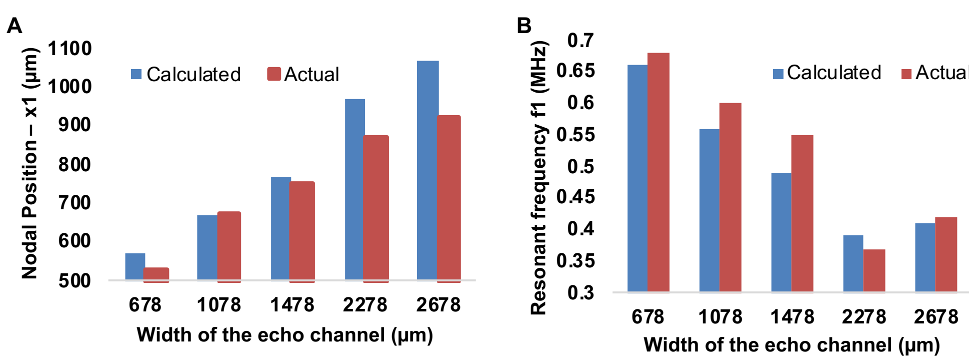

Fig. 2 **a** A graph showing the calculated and actual nodal positions when having different echo channel width. **b.** A graph of the expected and actual resonant frequencies. In all cases, the main channel widths remained constant (1600 μm wide)

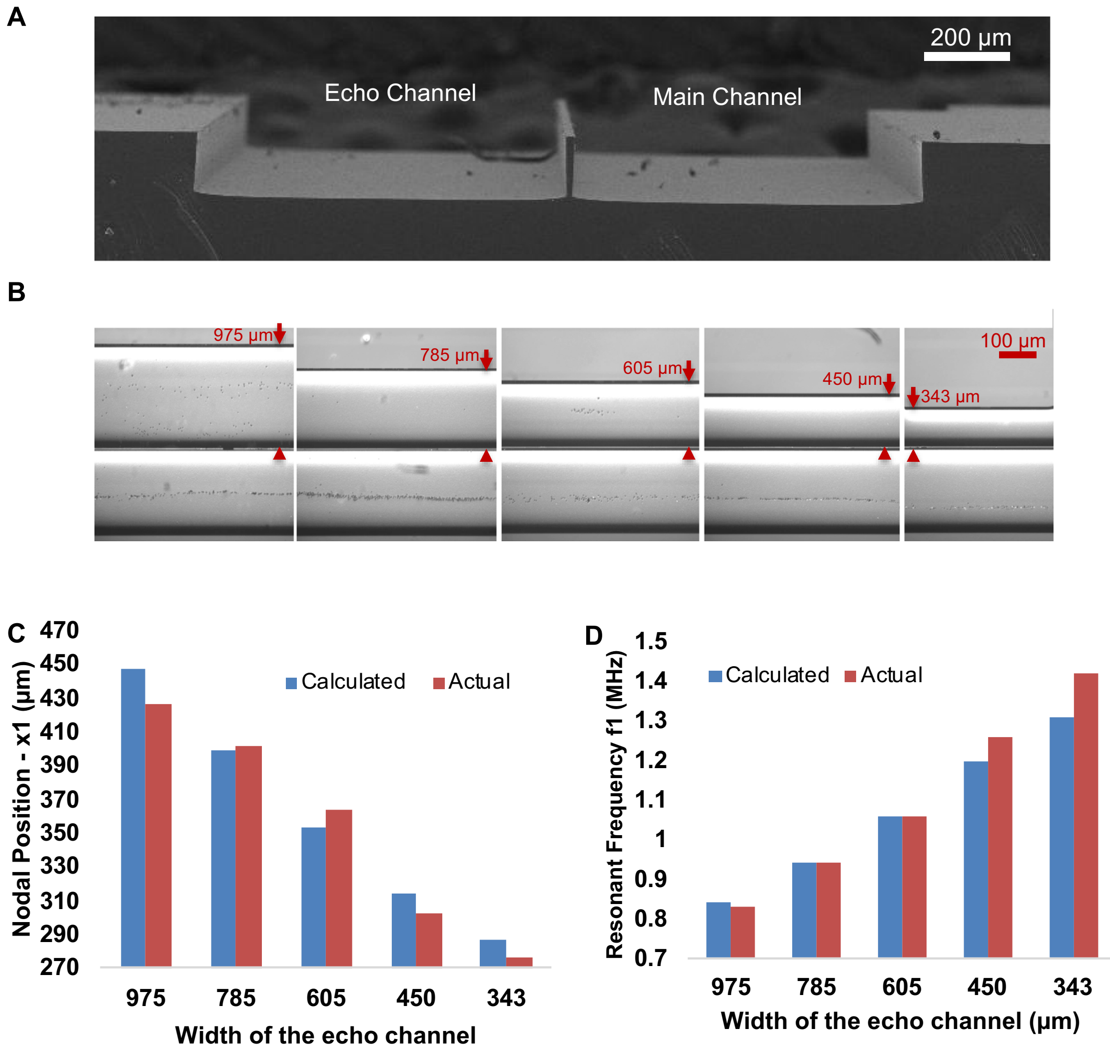

Fig. 3 **a** Cross-sectional SEM image of the etched silicon microchannel before anodic bonding with a glass cover substrate. The 10 µm wide thin wall that separates the main channel from the echo-channel can be clearly seen. **b** Bright field microscopic images (exposure time: 10 ms) showing particle positions within the main channel when the echo-channel width changes from 1075 µm to 343 µm (left to write, conditions summarized in Table 2). **c** A graph showing the expected and actual nodal positions. **d** A graph showing the expected and actual resonant frequencies that had to be applied to focus the particles in the main channel. In all cases, the main channel width is 800 µm and the separation wall thickness is 10 µm

Table 2 Summary of the various echo-channels tested and the corresponding parameters tested

Channel characteristics (µm)					Calc. freq (MHz)	Real freq (MHz) & Vpp
W_{main}	W_{echo}	W_{eff}	$Calc.x_1$	$Real\ x_1$	f_1	f_1
800	343	1148	287	276	1.31	1.42 (180 mV)
800	450	1257	314	302	1.20	1.26 (120 mV)
800	605	1413	353	364	1.06	1.06 (370 mV)
800	785	1595	399	402	0.94	0.94 (250 mV)
800	975	1787	447	426	0.84	0.83 (180 mV)

In all cases, the width of the main channel is 800 µm and the separation wall thickness is 10 µm nodal positions and required resonance frequencies compared to that of the calculated values. Another observation is that when the echo-channel width is equal to 450 µm, the minimum peak-peak voltage required to successfully focus the microspheres at one nodal plane is 120 mV and its resonant frequency is 1.26 MHz. When compared to the voltage required to focus particles in the other echo-channels, this voltage requirement is significantly lower. This is most likely due to the fact that the impedance of the PZT at that frequency is lower than the impedances at other frequencies.

In all cases, the width of the main channel is 800 µm and the separation wall thickness is 10 µm.

Adding an adjacent microfluidic echo channel next to the main microfluidic channel require that the separation wall thickness should be kept at minimum to reduce the loss of the acoustic waves traveling between the acoustic boundaries while avoiding leakage between two microfluidic channels. On the other hand, as seen from Table 2, when the width of the echo-channel is close or similar to the width of main microfluidic channel, the resonant frequencies match best with the expected values. However, as seen from both Table 1 and Table 2 there are some discrepancies between the expected and the actual values when the width of the echo-channel is very different from the width of main microfluidic channel. There can be multiple reasons why there is a discrepancy between the calculated nodal position and the real nodal position observed. One of the reasons could be that the wall thickness between the main fluidic channel and the echo-channel is uneven, or even though a fairly thin separation wall was utilized, some acoustic loss is still inevitable. Another reason could be the mismatch between the acoustic resonance frequency needed for the acoustofluidic device and the natural resonant frequency of the PZT used. But most importantly, the calculation does not account for the requirement of the voltage level to successfully move particles to the nodal positions. Different level of voltage applied may have different effect on the thin separation wall, and thus may affect the nodal position. Increased temperature level due to higher voltage applied can also affect the nodal position. Even though a cooling fan was successfully employed to limit the rise in temperature, a voltage beyond about 300 mV (applied to the amplifier) can easily result in more than 20 °C increase in temperature, which affect the sound velocity, thus the actual acoustic pressure nodal position.

Second, this discrepancy may be also attributed to the PZT transducer characteristics. PZT has its intrinsic electrical impedance, which is highly dependent on the applied frequency. The frequency at which the discrepancy between calculation and actual result is minimum (e.g., 878 and 2678 µm wide echo-channels), those frequencies were in line with the reported resonant frequencies of the PZT we used in our experiment (Arnold et al. 2015). If the driving frequency is away from this PZT resonance frequency, a higher voltage will be required to overcome the impedance of the transducer, thus affecting the nodal position as described in the previous paragraph. As summarized in Table 1 and Table 2 at some frequencies the PZT needed a higher voltage to actuate the acoustofluidic chip when compared to the other frequencies. This shows that the impedance of PZT might affect the acoustic actuation.

Through the experiments with the straight echo-channel devices, it was realized that as the driving frequency changes the electrical impedance of the PZT varies, which has a significant impact on the acoustophoretic force since the voltage level required to focus microparticles is an important factor on the acoustophoretic force. For instance, while testing one of the 1600 µm main flow channel devices, the applied frequency to the PZT was 0.6 MHz and the peak-to-peak voltage required to focus the microbeads was 460 mV, which was much higher than the voltage needed at 0.55 MHz where the echo-channel width was 1478 µm (Table 1). Similarly, when the applied frequency was 1.06 MHz, it required a peak-to-peak voltage of 370 mV, which is almost three times of the voltage required to focus the microbeads when the applied frequency was 1.26 MHz. This analysis shows that the required voltage to generate acoustic resonance is highly dependent on the applied frequency and the impedance of the PZT, as has been mentioned that electrical impedance of the PZT is dependent on the frequency (Cushing et al. 2017). To be able to generate an acoustic resonance without applying too high of a power that causes overheating issue, it is essential to overcome the impedance of the PZT with relatively low voltage. By taking this into account, a third design was created where the main channel width was 700 µm. While designing the echo-channels, some frequencies were avoided since they require high voltage to generate acoustic resonance based on the experimental results of straight echo-channel devices. Since those frequencies required higher voltages to generate acoustic resonance for particle focusing as shown in Table 1 and Table 2.

3.2 Staircase echo-channel device

The staircase echo-channel device was designed considering the acoustic resonance frequency mismatching issues identified through the first two devices. Two strategies were adopted. First, certain frequencies that require relatively high voltage to generate acoustic resonance based on the experimental results of straight echo-channel device were avoided. The PZT specification sheet showing the impedance of PZ26 piezoelectric transducer was utilized in selecting the frequency, and thus the echo-channel width. Taken together, the frequencies where the PZT impedance is relatively low, such as 1.49 MHz, 0.88 MHz, and 0.60 MHz were chosen as reference point to design the staircase echo-channel device. In addition, the resonant frequencies were selected where they could be applied as the sum of sinusoidal signals without requiring the dynamical change of frequency and applied voltage, so that multi-frequency acoustic field could be applied simultaneously easily. Based on these considerations, an echo-channel where its width changes step-wise along the flow direction as to change the nodal positions along the flow direction in a single acoustofluidic chip was designed. Figure 4a shows the illustration of a main flow channel (width: 700 µm) that has a neighboring staircase echo-channel composed of 3 different steps (i.e., echo-channel width: 300 µm, 1000 µm, 1800 µm). As seen from Fig. 4b, the location of the fluorescent microparticles flowing successfully changed from the upper part of the microfluidic channel towards the middle part of the microfluidic channel as the echo-channel width reduced along the flow direction.

Even though the frequency values matched well with the expected values as seen from Fig. 4d for the 700 µm-wide chip, the nodal position for the 300 µm-wide channel had a large difference compared to the other steps as shown in Fig. 4c. Since a significantly higher voltage of 800 mV had to be applied (Table 3), this may have resulted in overheating during the course of the experiment, requiring frequent re-tuning to maintain the microparticles.

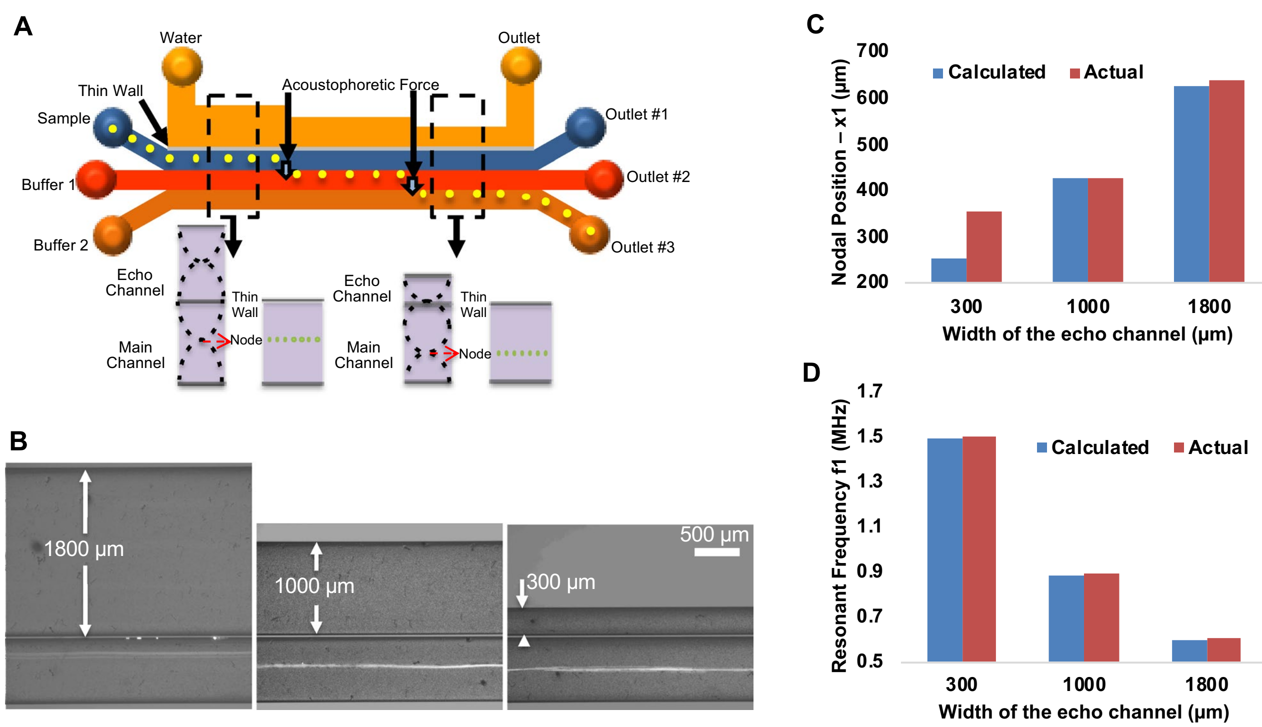

Fig. 4 **a** Illustration of the 3-step staircase echo-channel acoustic microfluidic device. **b** Microscope images showing fluorescent PS particles being focused to different pressure node positions when the echo-channel width changed from 1800 to 1000 and 300 µm (from left to right). Bright field images (10 ms exposure time) showing the microchannels were overlaid with the fluorescent images (400 ms exposure time) showing the fluorescent microbeads (white dots and white lines) to make visualization easy. The wall thickness separating the main microchannel from the echo-channel is 20 µm. **c** A graph showing the expected and actual nodal positions. **d** A graph showing the expected and actual resonant frequencies that had to be applied to focus the particles in the main channel. Main channel width = 700 µm

Table 3 Parameters and testing conditions for the staircase echo-channel device

Channel characteristics (µm)					Calc. freq (MHz)	Real freq (MHz) & Vpp
W_{main}	W_{echo}	W_{eff}	$Calc.x_1$	$Real\ x_1$	f_1	f_1
700	300	1004	251	356	1.49	1.50 (350 mV)
700	1000	1704	426	425	0.88	0.89 (230 mV)
700	1800	2504	626	638	0.60	0.61 (500 mV)

The width of the main channel is 700 µm and the wall thickness is 20 µm for all cases

The width of the main channel is 700 µm and the wall thickness is 20 µm for all cases. Overall, the nodal position change was ~ 280 µm, which is almost 40% of the main channel width. Even though the nodal position change when using the 1600 µm-wide channel was ~ 394 µm, this was less than 25% of the main channel width. Thus, for maximum tunability in terms of percent change of particle position in the main channel, the 700 µm-wide devices is ideal. However, if a particular application requires that the degree of position change in terms of absolute distance is important, a larger main channel width may be ideal. Besides that, footages with 500 µm-wide staircase acoustofluidic platform are provided as supplementary material. To provide further tunability to the nodal position in the main flow channel for a given microfluidic device already fabricated with a fixed echo-channel width, different liquid having different acoustic properties can be utilized as to change the speed of sound traveling through the echo channel medium. Such a concept has been previously demonstrated by Weinberger et al. (Jung et al. 2015). Thus, combining these two design aspects can provide further flexibility in tuning the acoustic nodal position in microfluidic channels.

In the present study, it was observed that the impedance of the piezoelectric transducer has an effect on actuation since the voltage required to overcome the electrical impedance of the transducer is strictly dependent on the frequency. First set of devices the main channel width was chosen as 1600 µm. However, this made frequency range narrow through different echo-channel widths. Because of that, second set of devices channel dimensions are reduced so that frequency range to be tuned to focus the microparticles was broadened. It is important to note that while actuating the acoustic microfluidic chips frequency selection needs to be considered so that overheating of acoustic microfluidic chips can be decreased by reducing the electrical impedance. As a summary, the idea of adding echo-channel next to the main fluidic channel was implemented and it was tried to optimize addressed how the problem of fixed-nodal position can be decreased by designing the channel geometries with appropriate parameters. Finally, a staircase echo-channel was designed, and this chip provided better capability in terms of changing the positions of acoustic pressure nodal positions inside the main fluidic channel.

4 Conclusion

Being contactless, label-free, and high-throughput, acoustofluidics particle and cell manipulation is preferable in many microfluidic applications as opposed to the other manipulation methods. However, because of their fixed acoustic nodal positions, cell and particle manipulation is also fixed to those nodal positions, somewhat limiting its applications. Some techniques are available that can provide more freedom to the particle manipulation location within a given channel, but none can change the position along the flow direction. To overcome this issue, here a staircase-shaped echo-channel located adjacent to the main channel and separated by a thin wall was designed. As the echo-channel width determines the location of the acoustic nodal position in the main flow channel, hence the position to which particles are focused to, the location of particles could be successfully tuned along the flow direction. It is expected that this new capability can open up additional application areas for acoustofluidic-based particle and cell manipulation.

Acknowledgement Sinan Yigit was supported by the Ministry of National Education of the Republic of Turkey. This work was also partially supported by the the National Research Foundation of Korea (NRF) Grant funded by the Korean government (No. NRF-2017R1D1A1B03029817).

References

Antfolk M, Laurell T (2019) Acoustofluidic Blood Component Sample Preparation and Processing in Medical Applications. In applications of microfluidic systems in biology and medicine Springer, Singapore, pp 1–25

Antfolk M, Magnusson C, Augustsson P, Lilja H, Laurell T (2015) Acoustofluidic, label-free separation and simultaneous concentration of rare tumor cells from white blood cells. Anal Chem 87(18):9322–9328

Arnold FJ, Gonçalves MS, Bravo-Roger LL, Mühlen SS (2015) Electric impedance of piezoelectric ceramics under acoustic loads. ECTI Trans Electr Eng Electron Commun 12(2):48–54

Cushing KW, Garofalo F, Magnusson C, Ekblad L, Bruus H, Laurell T (2017) Ultrasound characterization of microbead and cell suspensions by speed of sound measurements of neutrally buoyant samples. Anal Chem 89(17):8917–8923

Destgeer G, Cho H, Ha BH, Jung JH, Park J, Sung HJ (2016) Acoustofluidic particle manipulation inside a sessile droplet: four distinct regimes of particle concentration. Lab Chip 16(4):660–667

Ding, Xiaoyun, Sz-Chin Steven Lin, Brian Kiraly, Hongjun Yue, Sixing Li, I-Kao Chiang, Jinjie Shi, Stephen J. Benkovic, Tony Jun Huang (2012) "On-chip manipulation of single microparticles, cells, and organisms using surface acoustic waves." Proceedings of the National Academy of Sciences109, no. 28: 11105–11109.

Evander M, Nilsson J (2012) Acoustofluidics 20: Applications in acoustic trapping. Lab Chip 12(22):4667–4676

Fong EJ, Johnston AC, Notton T, Jung SY, Rose KA, Weinberger LS, Shusteff M (2014) Acoustic focusing with engineered node locations for high-performance microfluidic particle separation. Analyst 139(5):1192–1200

Fornell A, Nilsson J, Jonsson L, Periyannan Rajeswari PK, Joensson HN, Tenje M (2015) Controlled lateral positioning of microparticles inside droplets using acoustophoresis. Anal Chem 87(20):10521–10526

Haynes (2014) William M. CRC handbook of chemistry and physics. CRC press

Hopcroft MA, Nix WD, Kenny TW (2010) What is the Young's Modulus of Silicon? J Microelectromech Syst 19(2):229–238

Jung SY, Notton T, Fong E, Shusteff M, Weinberger LS (2015) Spatial tuning of acoustofluidic pressure nodes by altering net sonic

velocity enables high-throughput, efficient cell sorting. Lab Chip 15(4):1000–1003
Leibacher I, Schatzer S, Dual J (2014) Impedance matched channel walls in acoustofluidic systems". Lab Chip 14(3):433–610
Lenshof A, Magnusson C, Laurell T (2012) Acoustofluidics 8: Applications of acoustophoresis in continuous flow microsystems. Lab Chip 12(7):1210–1223
Park JW, Kim SH, Ito T, Fujii T, Kim SY, Laurell T, Lee SW, Goda K (2016) Acoustofluidic harvesting of microalgae on a single chip. Biomicrofluidics 10(3):034119
Pothuri C, Azharudeen M, Subramani K (2019) Rapid mixing in microchannel using standing bulk acoustic waves. Phys Fluids 31(12):122001
Wang H, Liu Z, Kim S, Koo C, Cho Y, Jang DY, Han A (2014) Microfluidic acoustophoretic force based low-concentration oil separation and detection from the environment. Lab Chip 14(5):947–956
Wang H, Liu Z, Shin DM, Chen ZG, Cho Y, Kim YJ, Han A (2018) Single-cell compressibility quantification for assessing metastatic potential of cancer cells through multi-frequency acoustophoresis. Microfluid Nanofluid 22(6):68
Wiklund M, Christakou A, Ohlin M, Iranmanesh I, Frisk T, Vanherberghen B, Önfelt B (2014) Ultrasound-induced cell–cell interaction studies in a multi-well microplate. Micromachines 5(1):27–49
Wiklund M, Günther C, Lemor R, Jäger M, Fuhr G, Hertz HM (2006) Ultrasonic standing wave manipulation technology integrated into a dielectrophoretic chip. Lab Chip 6(12):1537–1544
Yeo LY, Friend JR (2009) Ultrafast microfluidics using surface acoustic waves. Biomicrofluidics 3(1):012002